Ru-Promoted Ni/γAl₂O₃ Fluidized Catalyst for Biomass Gasification

Alan Rubén Calzada Hernandez [1], Daniel Gibran González Castañeda [1],
Adriana Sánchez Enriquez [1], Hugo de Lasa [2] and Benito Serrano Rosales [1,*

[1] Unit of Electrical Engineering, Universidad Autónoma de Zacatecas, Zacatecas 98160, Mexico;
alanosch@gmail.com (A.R.C.H.); dgibrangocas@hotmail.com (D.G.G.C.); adsaenr@yahoo.com (A.S.E.)

[2] Faculty of Engineering, Chemical Reactor Engineering Centre (CREC), Western University, London,
ON N6A 5B9, Canada; hdelasa@uwo.ca

* Correspondence: beniser@prodigy.net.mx; Tel.: +52-492-124-4456

Abstract: Fluidizable catalysts based on $Ni/\gamma Al_2O_3$ with added Ru were used for the gasification of a lignin surrogate (2-methoxy-4-methylphenol) in a fluidized CREC Riser Simulator reactor. This was done in order to quantify lignin surrogate conversion and lignin surrogate products (H_2, CO, CO_2 and CH_4) as well as the coke deposited on the catalyst. The catalysts that were evaluated contained 5% wt. Ni with various Ru loadings (0.25%, 0.5% and 1% wt). These catalysts were synthesized using an incipient Ni and Ru co-impregnation. Catalysts were characterized using XRD, N_2 adsorption-desorption (BET Surface Area, BJH), Temperature Programmed Reduction (TPR), Temperature Programmed Desorption (TPD) and H_2 chemisorption. Catalytic steam gasification took place at 550, 600 and 650 °C using 0.5, 1.0 and 1.5, steam/biomass ratios. The results obtained showed that Ru addition helped to decrease both nickel crystallite site sizes and catalyst acid site density. Moreover, it was observed that coke on the catalyst was reduced by 60%. This was the case when compared to the runs with the $Ni/\gamma Al_2O_3$ free of Ru.

Keywords: coke; nickel; ruthenium; gasification; tar; biomass

1. Introduction

In recent decades, biomass has received worldwide interest due to its great potential to substitute fossil fuels [1–3]. Biomass has several advantages given its abundance, renewability, and carbon-neutrality as well as its low sulfur content. It is a material mainly consisting of carbon, hydrogen, oxygen, nitrogen, and minerals [4–6]. Biomass can be converted using gasification and has zero net emissions of carbon dioxide. This can be achieved if the carbon dioxide released from the biomass is quantitatively recycled back into plants via photosynthesis [7].

Biomass steam gasification can produce a synthesis gas with a relatively high hydrogen content. This synthesis gas (CO + H_2) has diverse applications. It can be used for electricity production and for heat generation via direct combustion in internal combustion engines. It can also provide a valuable feedstock for the chemical industry to produce liquid hydrocarbon fuels and methanol [8,9].

In this respect, one can notice that gasifying lignocellulosic biomass produces CO, CO_2, H_2 and CH_4, as well as tar, char, ash and liquid materials. Tar production is particularly problematic, given that it causes fouling and blockage of process pipes, gas engines and gas turbines [10,11].

So far, different types of catalysts have been tested for tar conversion, such as calcined rocks, olivine, clay minerals, ferrous metal oxides, char, Fluid Catalytic Cracking (FCC) catalysts, alkali metal carbonates, activated alumina and supported metals [12–14]. However, supported Ni is the most commonly used catalyst given its high activity and given that it is comparatively inexpensive.

However, nickel catalytic activity may decrease over time due to sintering, sulfur poisoning, and especially, carbon formation. Carbon deposition may occur via several routes including methane dissociation, the Boudouard reaction, and the reaction between CO and H_2 [15].

When surface carbon containing species are formed over supported metal catalysts, they may be the result of the following: (a) carbon species condensation due to limited hydrogenation of hydrocarbons, or (b) surface species diffusion favoring carbon formation. Formed carbon may penetrate the metal crystallites, forming metal carbides.

Doping Ni with other elements has been shown to improve catalyst performance. For example, it has been reported that Pd increases and extends catalytic activity, as do Ru and Rh, which do not produce filamentous carbon. This is due to low carbon solubility in the metallic sites [16]. In addition, precious metal catalysts show superior activity and are, therefore, often used alone. Another advantage of using noble metal-based catalysts is that they are more resistant to oxidation, while Ni is more prone to being oxidized [16–20]. Zhang et al. calculated the activation energies on the Co catalysts for carbon diffusion, carbon accumulation, carbon hydrogenation and carbon penetration, using the density functional theory. Pt, Ru and B were considered as co-catalysts. On this basis, Pt and Ru were identified as facilitating C hydrogenation and inhibiting C diffusion, C accumulation and C penetration. [21].

Despite the fact that it has been reported that the addition of Ru helps with nickel reducibility and Ni° dispersion [22], an Ru–Ni–alumina catalyst has not yet been considered for tar derived from biomass steam gasification. To accomplish this, 0.25%, 0.5% and 1% wt. %Ru-5% Ni on a γ-Al_2O_3 catalyst were synthesized in the present study, via incipient co-impregnation followed by thermal decomposition of the Ru and Ni precursors. The synthesized fluidizable catalyst was characterized using several surface science techniques (BET Surface Area, XRD, Temperature Program Reduction (TPR), H_2 chemisorption). The prepared catalyst was evaluated under gasification conditions using a surrogate lignin tar compound (2-methoxy-4-methyl phenol) in a CREC Riser Simulator. The effect of various reaction conditions, such as temperature and steam/biomass mass ratio (S/B) on catalyst reactivity and coke formation were extensively studied. This showed the significant influence of the proposed Ru–Ni–alumina catalyst on coke reduction while converting a lignin surrogate (2-methoxy-4-methylphenol).

2. Biomass Gasification Reaction Network

Biomass gasification can be considered as a combination of primary and secondary reactions [7].

$$C_xH_yO_z + H_2O \overset{heat}{\to} H_2 + CO + H_2O + C_nH_{2n} + C_{(s)} + tars \tag{1}$$
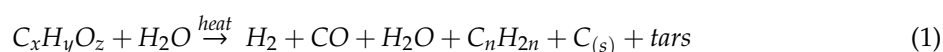
Secondary reactions break down superior hydrocarbons to produce permanent gases:

$$C_nH_{2n} + nH_2O \quad \to \quad nCO + (n+m)H_2 \tag{2}$$
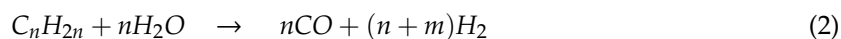
In addition, permanent gases can react changing the composition of the formed gases with this being a function of the selected gasifier conditions, as follows:
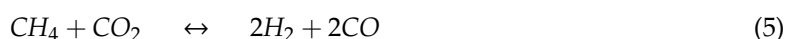
Water gas shift

$$CO + H_2O \quad \leftrightarrow \quad H_2 + CO_2 \tag{3}$$

Steam reforming of methane

$$CH_4 + H_2O \quad \leftrightarrow \quad 3H_2 + CO \tag{4}$$

Dry reforming of methane

$$CH_4 + CO_2 \quad \leftrightarrow \quad 2H_2 + 2CO \tag{5}$$

Char gasification

$$C + H_2O \quad \leftrightarrow \quad H_2 + CO \tag{6}$$

Boudouard reaction

$$C + CO_2 \quad \leftrightarrow \quad 2CO \tag{7}$$

Carbon hydrogenation

$$C + 2H_2 \quad \leftrightarrow \quad CH_4 \tag{8}$$

In spite of the tar gasification reaction network complexity, if active catalysts are used, Equations (1) and (2) may occur close to completion, while the other reactions (Equations (3)–(8)) may take place near chemical reaction equilibria.

3. Results and Discussion

3.1. Catalyst Characterization

Table 1 reports the BET surface area for the different catalysts prepared in the present study. It can be observed that the impregnation of the Ni onto the alumina support mildly decreases the support-specific surface area from 191 to 182.3 m^2/g. However, in catalysts with added Ru, the surface area increases slightly. These changes can be considered to be in the range of the expected specific surface area variations. Thus, there is little or no effect of the added Ni and Ru on the γAl_2O_3 surface area.

Table 1. Specific surface areas of the prepared catalysts (Cat).

Catalysts	S_{BET} (m^2/g)	Pore Size (A)
γAl_2O_3	191	110.2 ± 16
Cat A: 5%Ni/γAl_2O_3	182.3	108.4 ± 15
Cat B: 5%Ni-0.25%Ru/γAl_2O_3	190.7	105.6 ± 10
Cat C: 5%Ni-0.5%Ru/γAl_2O_3	194.8	100 ± 14
Cat D: 5%Ni-1.0%Ru/γAl_2O_3	194.9	104.6 ± 12

Furthermore, and with respect to the average pore size, one can also observe, in Table 1, a small average pore size decrease with Ni addition and a minor average pore size reduction with the additional Ru addition. These changes are in the range of the average pore size experimental error. Thus, these results points towards the consistent little effect of metal addition on the γAl_2O_3 support.

Figure 1a–d, report the Temperature Program Reduction (TPR) for the different catalysts of the present study. These figures also report, in all cases, the baseline used in TPR calculations (broken line).

Figure 1a reports the TPR for catalyst (Cat) A or 5% Ni/γAl_2O_3. Two TPR peaks at 307 and 488 °C were observed. The first peak was assigned to the thermal decomposition of the $Ni(NO_3)_2$ precursor, while the second peak was assigned to the NiO reduction with the H_2 leading to Ni formation [23]. Furthermore, and once the Ru was added, as shown in Figure 1b–d, one could observe a third early TPR peak. This early peak developed in the 235–239 °C range. This third early peak was assigned to RuO_3 reduction.

Table 2 describes the H_2 consumption and the percentages of Ni and Ru used for the prepared catalysts, as established with TPR. On this basis, one can make the following observations: (a) a 2.0–3.9 wt. % reducible Ni was observed by TPR, versus the 5wt. % nominal nickel; (b) Ru loadings were consistently in the anticipated range; (c) Ru addition appeared to contribute to a greater Ni reducibility.

One should note that hydrogen consumption for the catalyst of this study was calculated on the basis of NiO and RuO_3 precursor oxides. This was the case given the catalyst was pretreated with air at 600 °C prior to the TPR analysis. This assumption was consistent with the findings of others (Mazumder et al. [24], Sharma et al. [25]).

In addition, one can also see that the Ru influences the thermal decomposition and reduction in nickel peaks which occur at lower temperatures. For example, if one compares Cat C with 1 wt. % Ru

with Cat A with no added Ru, one can observe that the reduction temperature shifts from 307 to 250 °C (second peak) and from 488 to 389 °C (third peak). This variation of the reduction in temperature is assigned to a hydrogen spillover effect which lowers both the nickel nitrate precursor decomposition temperature and the NiO reduction temperature.
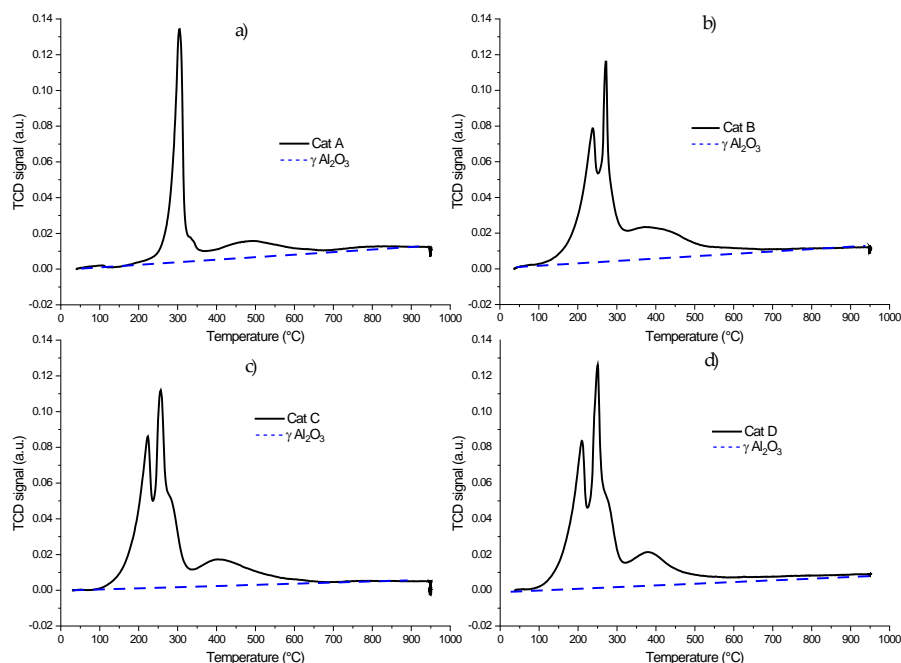

Figure 1. Temperature Program Reduction (TPR) using a 10v% H_2 in a He flow with a 50 °C/min ramp for: (**a**) Fresh Cat A: 5% Ni/γAl$_2$O$_3$, (**b**) Fresh Cat B: 5% Ni- 0.25%Ru/γAl$_2$O$_3$,(**c**) Fresh Cat C: 5% Ni-0.5%Ru/γAl$_2$O$_3$, (**d**) Fresh Cat D: 5% Ni- 1.0%Ru/γAl$_2$O$_3$.

Table 2. Hydrogen consumption with the percentage of reducible Ni and Ru.

Catalysts	H_2 Consumption (cm^3/g STP)	Reducible Ni (wt. %)	H_2 Consumption (cm^3/g STP)	Reducible Ru (wt. %)
Cat A: 5%Ni/γAl$_2$O$_3$	7.73	2.02		
Cat B: 5%Ni-0.25%Ru/γAl$_2$O$_3$	10.12	2.71	2.2	0.33
Cat C: 5%Ni-0.5%Ru/γAl$_2$O$_3$	12.07	3.16	3.21	0.48
Cat D: 5%Ni-1.0%Ru/γAl$_2$O$_3$	14.86	3.89	4.13	0.77

Furthermore, the surface morphologies of the various catalysts of this study were investigated using scanning electron spectroscopy (SEM), as shown in Figure 2. The SEM pictures show the minimum agglomeration of the 5% Ni/γAl$_2$O$_3$ alumina particles as well as the minimum agglomeration of the 5% Ni-0.25% Ru/γAl$_2$O$_3$ alumina particles.

Figure 3 reports the catalyst particle size distribution with 58.6 μm being the average catalyst particle size. These alumina particles belong to Group B of the Geldart Classification and display adequate particle sizes for good fluidization in the CREC Riser Simulator.

Moreover, one can observe that Ru addition affects neither the surface morphology nor the particle size distribution. The average particle size remains at 54.6 μm for the 5% Ni-0.25% Ru/γAl$_2$O$_3$ catalyst as reported in Table 3.

Table 3 also reports the Ni loading in the outer alumina fluidizable particles' one micron-thick shell, as determined with EDX. It is interesting to note that the observed EDX Ni loading is close to the nominal 5 wt. % Ni loading. These EDX results also provide a strong indication that the added metals, using incipient wetness impregnation, were uniformly distributed across the 60-micron particles.
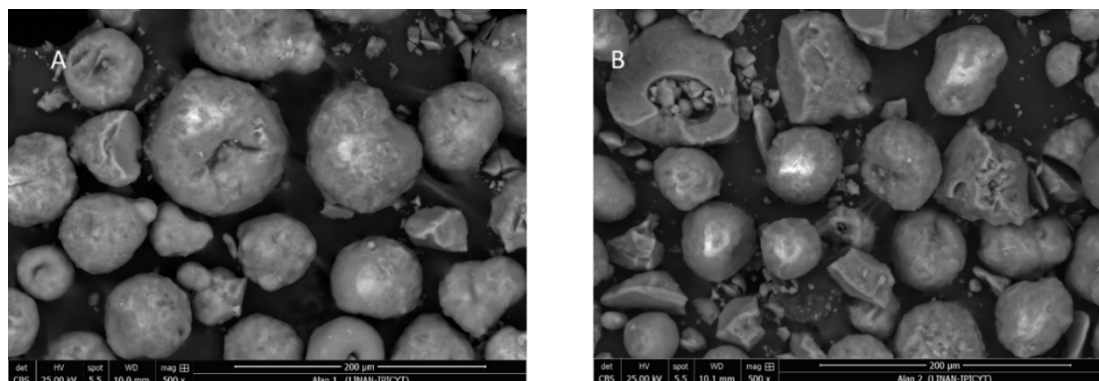
Figure 2. SEM image for (**A**) 5% Ni/γAl₂O₃ and (**B**) 5% Ni-0.25% Ru/γAl₂O₃.
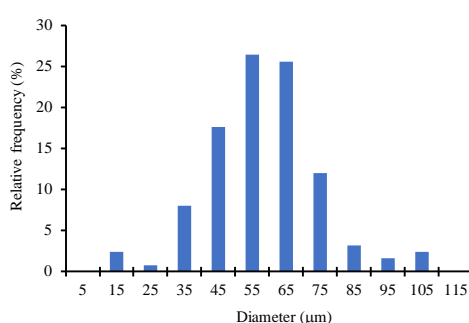

Figure 3. Particle size distribution of the catalyst 5%Ni/γAl₂O₃.

Table 3. Particle size and nickel loading.

Catalyst	Particle Size (μm)	wt. % of Ni
Cat A: 5%Ni/γAl₂O₃	58.6	5.7
Cat B: 5%Ni-0.25%Ru/γAl₂O₃	54.6	4.2

Furthermore, and regarding the catalyst acid sites, they were measured using ammonia TPD peaks. Figure 4 describes the desorption profiles for the different catalysts of the present study.

Table 4 shows the distribution of the acid sites, which were classified in two groups: (a) weak strength sites or sites displaying NH_3 desorption peaks in the 25–200 °C range and (b) medium strength sites or sites involving NH_3 desorption peaks in the 200–400 °C range. Given that peaks overlapped, TPD peaks were deconvoluted using Gaussian functions.

Table 4 shows that the medium strength acid sites are, in all cases, the most abundant ones. In this respect, it was also possible to observe that the nickel addition reduces the ammonia desorption peaks from 192.4 μmole/g for γ-Al₂O₃ to 149.3 μmole/g for 5%Ni/γAl₂O₃. Furthermore, it can also be noticed that Ru addition together with Ni, decreases further the medium and weak acid sites. This is desirable given the significant role of acid sites on coke formation [24,26].

Figure 5 reports the diffractograms for the γAl₂O₃ support and for the Ni-γAl₂O₃ with different Ru loadings. While it is possible to observe the characteristic γ alumina support peaks at 37.5°, 45.9° and 66.9° [13], the peaks for the γ alumina loaded with Ni and Ru could not be seen. This was assigned to the low levels of both Ni and Ru.
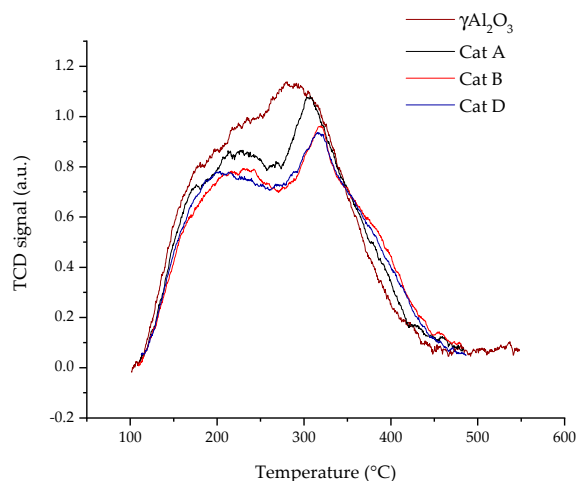
Figure 4. TPD profiles for the γAl_2O_3 support with different catalyst loadings: Cat A: 5% Ni/γAl_2O_3, Cat B: 5% Ni-0.25%Ru/γAl_2O_3, Cat C: 5% Ni-0.5%Ru/γAl_2O_3, Cat D: 5% Ni-1.0%Ru/γAl_2O_3.

Table 4. Distribution of acid sites.

Catalyst	Acid Sites (μmole/g)		
	Weak (25–200 °C)	Medium (200–400 °C)	Total
γ-Al$_2$O$_3$	42.3	192.4	234.7
Cat A: 5%Ni/γAl_2O_3	64	149.3	213.3
Cat B: 5%Ni-0.25%Ru/γAl_2O_3	54.6	138.7	193.3
Cat D: 5%Ni-1.0%Ru/γAl_2O_3	54.3	136	190.3

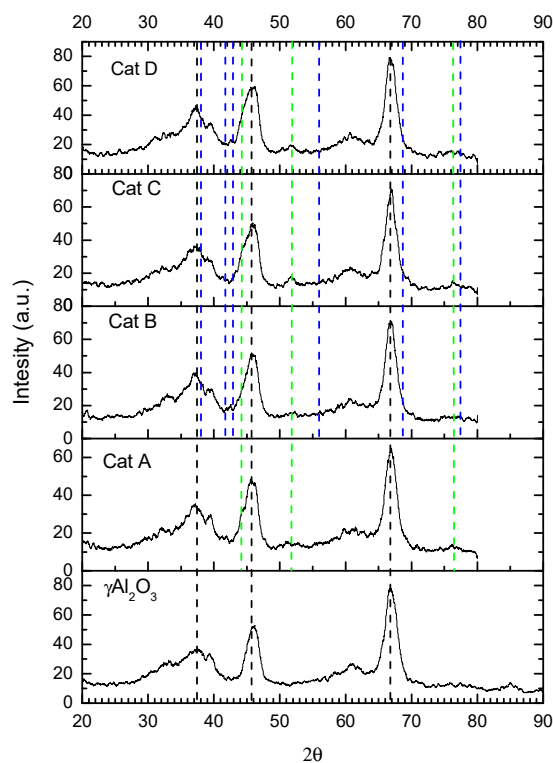**Figure 5.** XRD diffractograms for various catalysts studied: γAl_2O_3 peaks (identified with black vertical dashed lines), Ni on γAl_2O_3 peaks (identified as green vertical dashed lines), (c) Ru on γAl_2O_3 peaks (identified with blue vertical dashed lines). Codes: Cat A: 5%Ni/γAl_2O_3, Cat B: 5%Ni-0.25%Ru/γAl_2O_3, Cat C: 5%Ni-0.5%Ru/γAl_2O_3; Cat D: 5%Ni-1%Ru/γAl_2O_3.

Table 5 summarizes the results obtained using H_2 chemisorption. On this basis, it can be observed that the percentual metal dispersion increases up to 8.7% at the lowest 0.25 wt. % Ru loading. Consistent with this, the crystallite sizes decrease with Ru addition, achieving a minimum value of 9.7 nm.

Table 5. Metal dispersion and nickel crystallite sizes.

Catalysts	Metal Dispersion (%)	Ni–Crystallite Size (nm)
Cat A: 5%Ni/γAl$_2$O$_3$	3.9 ± 0.1	21.7 ± 0.54
Cat B: 5%Ni-0.25%Ru/γAl$_2$O$_3$	8.7 ± 0.1	9.7 ± 0.7
Cat C: 5%Ni-0.5%Ru/γAl$_2$O$_3$	5.9 ± 1.2	14.38 ± 2.9
Cat D: 5%Ni-1.0%Ru/γAl$_2$O$_3$	5.1 ± 0.1	16.5 ± 0.33

3.2. Gasification Results

Lignin is a main biomass carbohydrate constituent. Typically, lignin content in biomass ranges from 49.7 to 77.5 wt %. Lignin is a polymer displaying similar chemical functionalities as 2-methoxy-4-methylphenol (2M4MP). It was on this basis that the 2M4MP was chosen as a surrogate compound to study the gasification of tar derived from biomass gasification. The performance of the different Ni and Ni–Ru γAl$_2$O$_3$ supported catalysts was evaluated in a CREC Riser Simulator using steam and 2M4MP at 600 °C, 20 s reaction time, catalyst/2M4MP (Cat/2M4MP) ratio of 2.663 g/g and a steam/2M4MP (S/2M4MP) ratio of 1.5 g/g.

Table 6 reports the 2M4MP gasification conversions at 600 °C, with and without a catalyst being present. One can see that there is an important increase in 2M4MP conversion from 50% to 80% when catalysts are used.

Table 6. 2M4MP conversion during thermal and catalytic runs at 600 °C in the CREC Riser Simulator. S/2M4MP = 1.5 g/g, Cat/2M4MP = 2.63g/g.

Experiment	2M4MP Conversion (%)
Thermal runs	50 ± 5.5
Catalysts A,B,C,D	80 ± 3.5

Figure 6 reports the mole fractions of the gas products and the C_6–C_8 hydrocarbons (78–137 g/mole molecular weight) obtained with the different prepared catalysts. These mole fractions can also be compared with the ones predicted using chemical equilibrium calculations and the ones from thermal conversion (experiments without the catalyst present).

Furthermore, while reviewing Figures 6 and A1 from Appendix A, one can also observe the significantly reduced C_6–C_8 fraction (78–137 g/mole molecular weight) when dealing with 2M4MP catalytic gasification.

It can be observed in Figure 6, that for all catalysts studied, there is a significant influence of the forward methane reforming reaction (Equation (4)), without the corresponding backward reaction compensation. This yields a methane mole fraction significantly below equilibrium values. In Figure 6, one can also observe that ruthenium addition has a beneficial effect on hydrogen formation with the H_2 mole fraction increasing by 10.2%. One can also see that Ru diminishes CO_2 mole fractions by an average of 7.7%. Furthermore, and if one compares the hydrogen mole fractions obtained from the prepared catalysts with those with added Ru (Cat B, Cat C and Cat D), one can see that there is no significant difference between them.

One should also notice that the prepared catalysts are stable in terms of their catalytic activity. This is the case given that, after five consecutive 2M4MP/water injections in the CREC Riser Simulator, there was no noticeable catalyst activity decay (+/−3%). Thus, no regeneration was effected between consecutive runs, with the coke formed being evaluated at the end of the fifth consecutive run using TOC. Given the observed catalyst stability, it is speculated that coke forms mainly on the alumina support and not on the Ni–Ru crystallites.
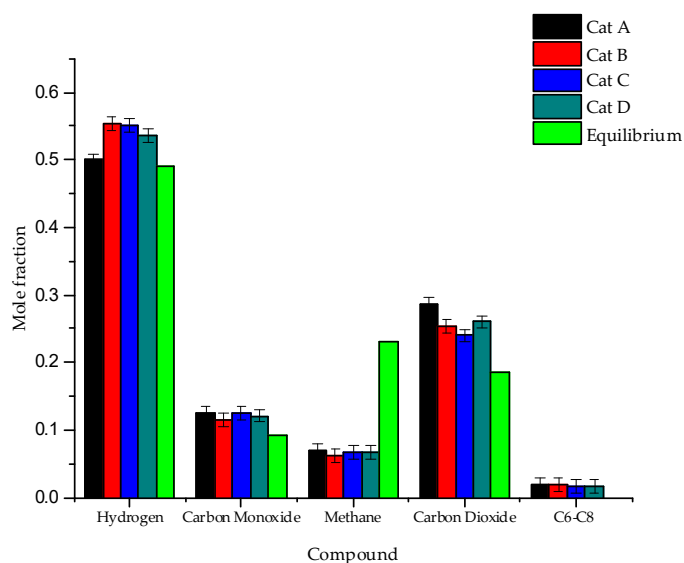
Figure 6. Mole fractions of the gasification products on a dry basis. Different catalysts are evaluated using a 2M4MP model compound at: S/2M4MP = 1.5 g/g; Cat/2M4MP = 2.63g/g; reaction time = 20 s, temperature = 600 °C. Codes: (a) Cat A: 5%Ni/γAl$_2$O$_3$, Cat B: 5% Ni-0.25%Ru/γAl$_2$O$_3$; Cat C: 5% Ni-0.5%Ru/ γAl$_2$O$_3$; Cat D: 5% Ni-1%Ru/ γAl$_2$O$_3$, (b) reported values are the average of at least three repeats.

Figure 7, reports the percentage of coke deposited on the catalysts, as measured by Total Organic Carbon (TOC), and after the fifth 2M4MP/steam consecutive injection. Coke selectivity is defined as the ratio of grams of coke being deposited on the catalyst over the grams of 2M4MP carbon converted.
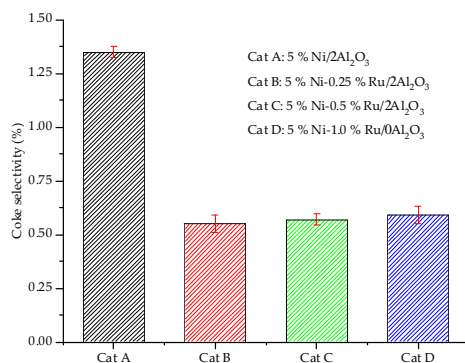

Figure 7. Coke selectivity during 2M4MP catalytic gasification. Conditions: S/2M4MP = 1.5 g/g; Cat/2M4MP = 2.63g/g; reaction time = 20 s, temperature = 600 °C. Note: reported values are the average of at least three repeats.

One can observe, in Figure 7, the significant reduction in coke once the Ru is added to the prepared catalysts. This can be attributed to the Ru's role in promoting both char gasification (C+H$_2$O → CO+H$_2$) and the Boudouard reaction (CO$_2$ + C → 2CO). Additionally, this is in line with both an increased hydrogen and increased mole fractions. This is the case when Ru doped catalysts are used, as shown in Figure 6.

Regarding the reduced coke formation on Ru doped catalysts, one can anticipate this effect given the ammonia TPDs, as reported in Table 4. Table 4 shows that, with Ru addition, there is a reduction in weak and medium strength acid site density, which appears to enhance coke formation. Moreover, consistent with TPD results, one can see that higher Ru levels on the catalysts have little effect on medium strength acid site's density, leading to unchanged coke yields.

Thus, and given that higher Ru levels have no influence on coke yields and hydrogen yields, the lowest Ru loading (0.25%) was selected to develop further gasification runs. During these runs, the following conditions were changed systematically: (a) catalyst loading; (b) reaction temperature; (c) steam/2M4MP ratio. To accomplish this, runs were carried out in the CREC Riser Simulator using 50, 100 and 150 mg of catalyst.

Figure 8 reports the average product mole fractions obtained using Cat A: 5%Ni/γAl$_2$O$_3$ and Cat B: 5%Ni/γAl$_2$O$_3$.
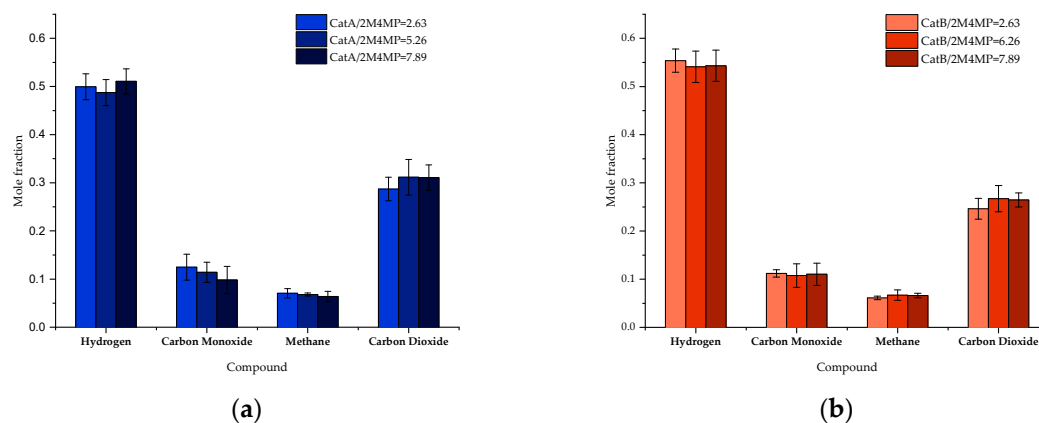
Figure 8. Mole fractions of the products on a dry basis using (**a**) Cat A: 5%Ni/γAl$_2$O$_3$ and (**b**) Cat B: 5%Ni/γAl$_2$O$_3$, with different catalyst loadings. Conditions: S/2M4MP = 1.5 g/g, 20 s reaction time, temperature = 600 °C. Note: reported values are the average of at least three repeats.

It can be observed, in Figure 8, that there is no significant change in the distribution of the product mole fractions with respect to amount of catalyst used. Thus, one can conclude that the lowest Cat/2M4MP ratio is adequate for the obtained 2M4MP high conversions and desired product distribution.

Figure 9 reports the coke selectivity during the catalytic steam gasification of 2M4MP using different catalyst loadings.
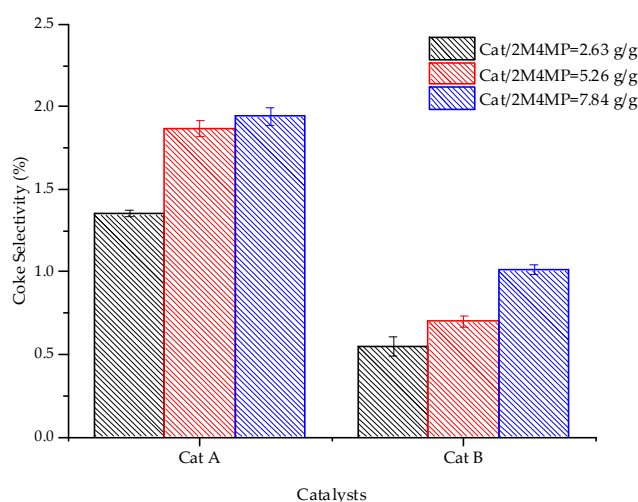

Figure 9. Coke selectivity during 2M4MP gasification using Catalyst A: 5% Ni/γAl$_2$O$_3$ and Catalyst B: 5% Ni-0.25%Ru/γAl$_2$O$_3$. Conditions: steam/2M4MP = 1.5 g/g; reactions time: 20 s; temperature = 600 °C. Reported values are the average of at least three repeats.

Thus, Figure 9 shows that Cat B with added Ru consistently displays, for various steam/2M4MP ratios, lower coke selectivity (g coke/g 2M4MP converted) than Cat A catalysts with no Ru addition. This consistent trend for Cat B allows one to anticipate a better catalytic stability for catalysts with added Ru.

Figures 10 and 11 also report coke selectivity for Cat A and Cat B at different catalyst loadings, as a function of temperature. Experiments were carried out at several S/2M4MP ratios and with a 2.63 Cat/2M4MP ratio. One can see that, for all cases, the coke selectivity decreases at higher thermal levels. One can also notice that the coke selectivity for Cat B (Figure 11) is approximately 50% lower than that for Cat A, with this being true for all temperatures and S/2MMP ratios studied.
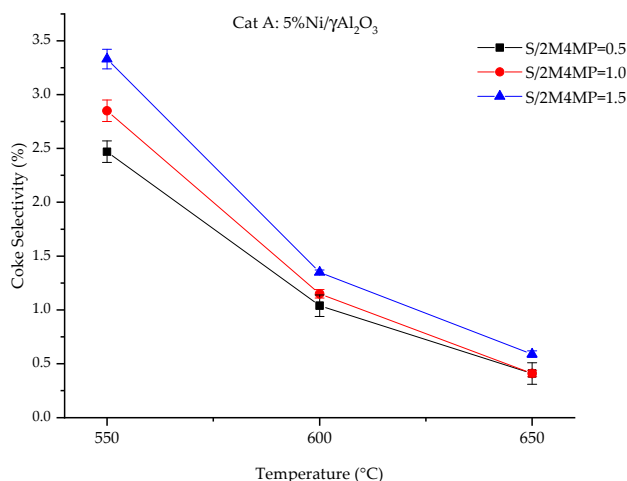

Figure 10. Coke selectivity for Cat A ($5\%Ni/\gamma Al_2O_3$). Using 2-Methoxy-4Methyl Phenol as a surrogate model compound for gasification. Note: reaction time: 20s. Reported values are the average of at least three repeats.
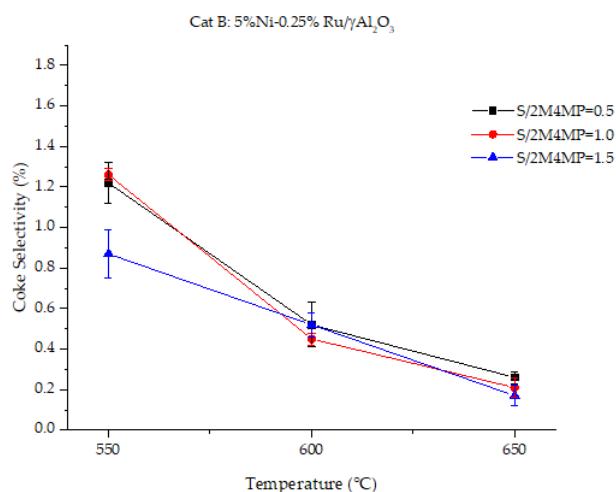

Figure 11. Coke selectivity for Cat B ($5\%Ni-0.25\%Ru/\gamma Al_2O_3$) Using 2-Methoxy-4Methyl Phenol as a surrogate model compound for gasification. Note: reaction time: 20s. Reported values are the average of at least three repeats.

One interesting and consistent issue with both Cat A and Cat B ($5\% Ni/\gamma Al_2O_3$ is the significant effect of S/2M4MP ratios on coke selectivity at 550 °C. This influence occurs, however, at 600 and 650 °C. Thus, on this basis, one can consider that there is an increased influence of coke steam reforming ($C + H_2O \rightarrow CO + H_2$) at the higher thermal levels.

Figure 12 compares the experimental mole fractions obtained with Cat A with those predicted at chemical equilibrium for 2M4MP gasification at 600 °C and with different S/2M4MP ratios. One should mention that chemical equilibrium calculations were developed following the procedure reported in Salaices et al. [7], which accounts for various reactions, as described in Equations (6) to (8).

Furthermore, Figure 13 reports the experimentally observed product mole fractions for Cat B, with chemical equilibrium values during the steam gasification of 2M4MP, at different temperatures.

Thus, in Figures 12 and 13, one can consistently see that Cat B yields higher hydrogen mole fractions, with this being true for the three S/2M4MP ratios and three thermal levels. In this respect, the hydrogen values obtained, which supersede chemical equilibrium values, point to the catalytic 2M4MP conversion. These hydrogen values remain moderately affected by the chemical equilibrium of the secondary gasification reactions (Equations (6)–(8)).

Furthermore, and consistent with this, one can observe that Cat B yields a smaller methane mole fraction than Cat A, with both mole fractions well below chemical equilibrium values. Finally, one can notice higher CO and CO2 mole fractions for both Cat A and Cat B than chemical equilibrium values, with this being consistent with the catalyst-promoted methane reforming and water–gas shift reactions.

In summary, the Cat B developed in the present study promises to be valuable for biomass-derived tar gasification. This is given the high H_2 mole fractions obtained, the significantly reduced coke formed and the important C_6–C_8 decrease.
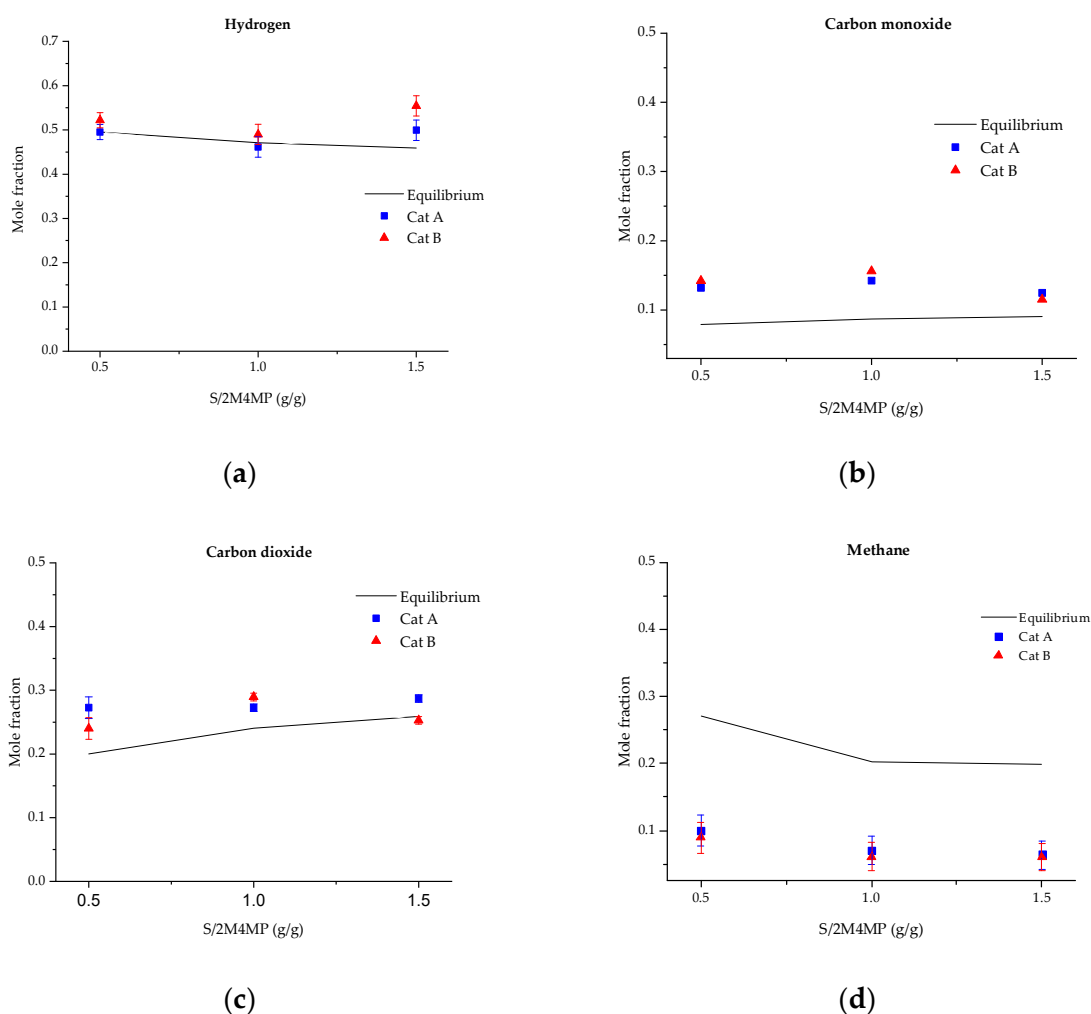

Figure 12. Product mole fractions (**a**) Hydrogen, (**b**) Carbon monoxide, (**c**) Methane, (**d**) Carbon dioxide on a dry basis at different ratios of S/2M4MP, using Cat A: 5%Ni/γAl$_2$O$_3$, Cat B: 5%Ni-0.25%Ru/γAl$_2$O$_3$. The solid line represents the equilibrium data. (T = 600 °C; Cat/B = 2.63 mg; 20 s reaction time). Reported values are the average of at least three repeats.
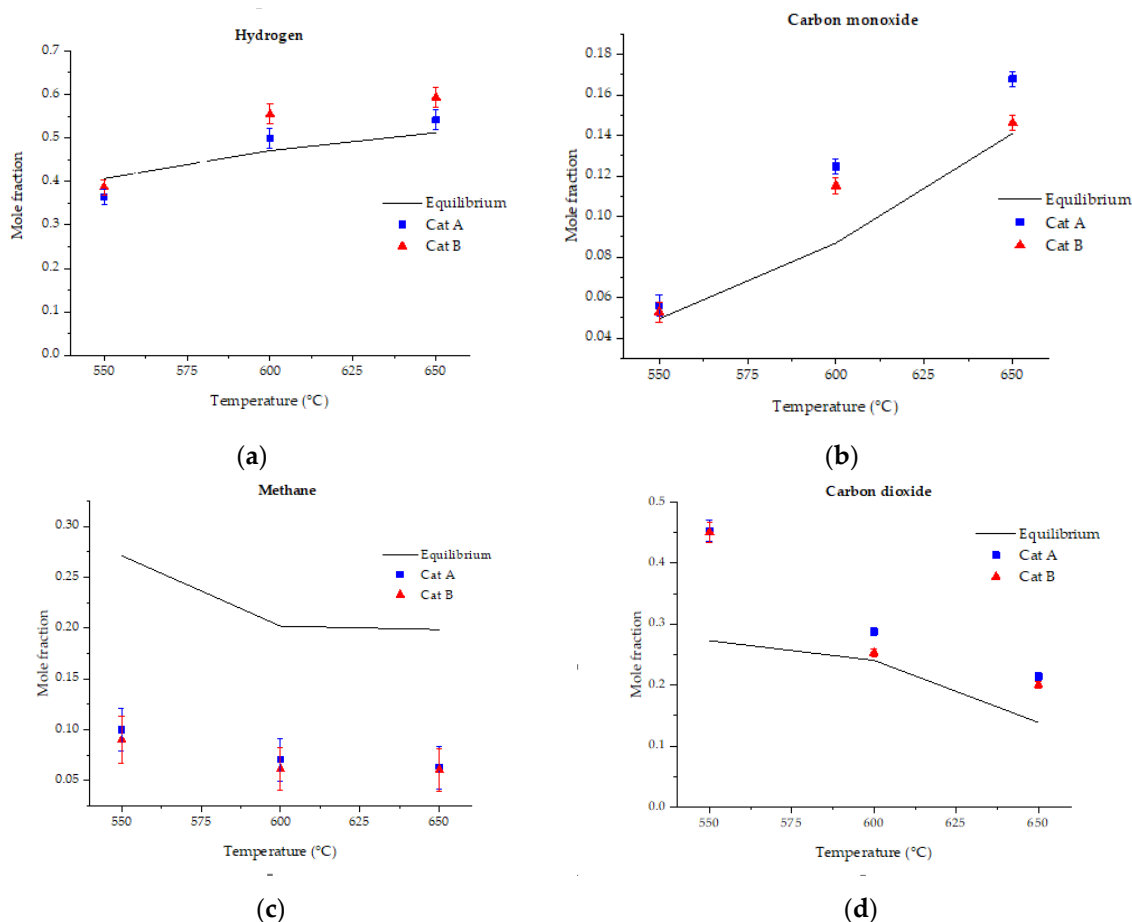
Figure 13. Product mole fractions (**a**) Hydrogen, (**b**) Carbon monoxide, (**c**) Methane, (**d**) Carbon dioxide from gasification on a dry basis at different temperatures using Cat A: 5%Ni-5%Ru/γAl$_2$O$_3$ and Cat B: 5%Ni-0.25%Ru/γAl$_2$O$_3$. The solid line represents the equilibrium data (S/2M4MP = 1.0; Cat/B = 2.63 mg; 20 s reaction time). Reported values are the average of at least three repeats.

4. Materials and Methods

4.1. Catalysts Preparation

Ni-based (Ni–Ru/γAl$_2$O$_3$) catalysts were prepared using a specially designed incipient wetness technique. This involved a one-step impregnation, with the direct reduction in metal precursors after each impregnation of fluidizable support. A fluidizable γAl$_2$O$_3$ support (Sasol Catalox SSCa5/200, North America Inc., Houston, T.X., USA.) was used as a catalyst support. Ni(NO$_3$)$_2$ 6H$_2$O (CAS 13,478-00-7) and RuCl$_3$ from Sigma Aldrich (Toluca, Mexico) were employed as chemical precursors to reach the desired metal loading.

Three main steps were involved in the catalyst preparation: (a) support impregnation, (b) drying, and (c) metal precursor reduction. For Cat A with 5% w/w Ni, an Ni(NO$_3$)$_2$ 6H$_2$O solution in deionized water solution was added, drop by drop, to the alumina support under stirring and vacuum conditions. In the case of the catalysts with added Ru, a solution was prepared with the two precursors: Ni(NO$_3$)$_2$ 6H$_2$O and RuCl$_3$. In the case of the catalysts with added Ru, a solution was prepared with the two precursors: Ni(NO$_3$)$_2$·6H$_2$O and RuCl$_3$. Three solutions were prepared for the three consecutive impregnation steps to obtain the 5% Ni-0.25% Ru, 5% Ni-0.5% Ru and 5% Ni-1.0% Ru catalysts. In between steps, the catalyst samples were dried at 100 °C to prevent water saturation. After the impregnation of precursor solutions, the resulting paste was dried slowly at 230 °C overnight. The dried powder was then reduced in a specially designed fixed bedchamber at 600 °C for 5 h under the flow of H$_2$.

4.2. Catalyst Characterization

BET analysis was employed to establish the specific surface area, the average pore radius and pore volume of the prepared catalyst samples. With this end in mind, a Micromeritics 2720 instrument (Norcross, GA, USA) allowed N_2 adsorption at 77 K. A 0.2 mg catalyst sample was employed in each analysis, being degassed prior to the analysis at 573 K during 2.5 h.

SEM was effected using a Field Electron and Ion Company-FEI Helos Nanolab 600 unit (Hillsboro, O.R., USA.). To avoid sample charging effects, catalysts were coated with a conductive carbon film. Then, the SEM was run using an accelerating voltage of 30 keV. EDX for the various catalysts was obtained in the same equipment, to establish Ni loading in the outer particle surface.

TPR runs were conducted in a Micromeritics 2720 unit (Norcross, GA, USA) using 25–30 mg catalyst samples. Every catalyst sample was preheated first for line conditioning, under 50 mL/min nitrogen flow for a 30 min period. Then, the temperature was increased up to 250 °C and held for 30 min. This allowed the removal of moisture from the sample, the sample holder and the connecting lines. Following this, $10\%H_2/90\%Ar$ at rate of 50 mL/min was introduced and the temperature was increased to 950 °C at a 10 °C/min rate. The hydrogen uptake was recorded using a Thermal Conductivity Detector (TCD, Micromeritics, Norcross, GA USA)).

TPD-NH_3 profiles were obtained using a Micromeritics 2720 unit (Norcross, GA, USA). To accomplish this, 100 mg of each catalyst was pretreated with a flow of hydrogen at 600 °C for 20 min. After that, the sample was cooled down to 100 °C under an inert gas flow. When the 100 °C temperature was reached, a 5% NH_3 in He gas contacted the sample for 60 min. Then, a 50 cm^3/min He carrier gas contacted the catalyst sample, with the temperature being increased from 100 to 500 °C, at a temperature ramp of 10 °C/min. Desorbed NH_3 was measured using a thermal conductivity detector Micromeritics, Norcross, GA, USA).

The metal dispersion and average crystallite sizes were calculated using H_2 chemisorbed at 50 °C, following catalyst sample reduction via TPR. The H_2 chemisorption involved 20 consecutive H_2 pulses injected into an argon flow until catalyst saturation was reached.

X-ray powder diffraction patterns was obtained on a Rigaku Miniflex Diffractometer (Auburn Hills, M.I., USA) using Ni filtered Cu Kα (λ = 0.15406 nm) radiation. The samples were scanned every 0.02° from 20 to 90°, with a scan time constant of 2°/min.

4.3. CREC Riser Simulator

The steam gasification of 2-methoxy-4-methylphenol (a lignin surrogate) was performed using a CREC Riser Simulator (Recat Technologies Inc., London, Ontario, Canada) which is a bench-scale mini-fluidized bed reactor with a volume of 50 cm^3. The Riser Simulator is specially designed for catalyst evaluation under controlled conditions of temperature and initial pressure.

The Ni catalysts, already thermally treated during the preparation process, were loaded into the catalyst basket. The reactor system was sealed, leak tested and heated to the reaction temperature under an argon or helium atmosphere. Then, the feed was injected, and once the reaction time was reached, the reaction products were evacuated from the reactor to the vacuum box. Reactor and vacuum box pressure data against time were recorded by the Personal Daq Acquisition Card. After the reaction, the products were analyzed by the GC system (Shimadzu, Nakagyo-ku, Kyoto, Japan),, equipped with two capillary columns in parallel: Agilent Technologies CP 7430 for permanent gases and Molsieve for CO_2 analysis. The columns were connected to a Thermal Conductivity Detector (TCD) in series with a Flame Ionization Detector (FID) (Shimadzu, Nakagyo-ku, Kyoto, Japan). To compare the performance of the prepared catalysts, gasification experiments were performed at 550, 600 and 650 °C using steam/biomass ratios of 0.5, 1.0 and 1.5 with a catalyst/2M4MP ratio of 2.63 g/g and 20 s reaction time.

The catalysts studied were evaluated through five consecutive reactions without regeneration in between them. This allowed one to assess catalyst stability by measuring both catalyst activity and coke formation.

5. Conclusions

(a) The Ru-promoted Ni catalyst supported on γAl_2O_3 of the present study is suitable for lignin surrogate steam gasification, displaying an 80% 2M4MP conversion at 600 °C in a CREC Riser Simulator;

(b) The 5% Ni-0.25% Ru/γAl_2O_3 catalyst displays adequate physicochemical properties in terms of specific surface areas (larger than 190 m^2/g), reducible nickel (bigger than 3%), reducible ruthenium (bigger than 3%) and a decrease of acidity by 6%, with metal addition;

(c) The addition of Ru increases Ni reducibility (34%) on the catalyst and promotes, as a result, an Ni spillover;

(d) The Ru on Ni/γAl_2O_3 catalyst reduces coke selectivity (60%), with this being more significant at the higher temperatures studied. This indicates that Ni with added Ru likely promotes char gasification and the Boudouard reaction. This was consistent with the acid site reduction observed with Ru addition;

(e) The H_2, CO_2 and CO yields remain for all catalysts studied, at supra-equilibrium levels with methane remaining, however, significantly below chemical equilibrium. This finding is assigned to the significant role of methane reforming;

(f) A Ru addition above 0.25 wt. % Ru does not improve further hydrogen mole fractions but decrease in CO_2;

(g) Increased loading of Cat A (5% Ni/γAl_2O_3) and Cat B (5% Ni-0.25% Ru/γAl_2O_3) in the CREC Riser Simulator leads to unchanged gas phase product fractions, only slightly increasing the coke deposited;

(h) For both Cat A (5% Ni/γAl_2O_3) and Cat B (5% Ni-0.25% Ru/γAl_2O_3), the temperature effect on product mole fractions is similar with the water–gas shift reaction and methane reforming, leading to a CO_2 reduction and a CO increase.

Appendix A. 2M4MP Thermal Gasification

Figure A1 reports the mole fractions of the gas products, as well as the C_6–C_8 hydrocarbon (78–137 g/mol molecular weight) fractions obtained in the 2M4MP thermal runs.
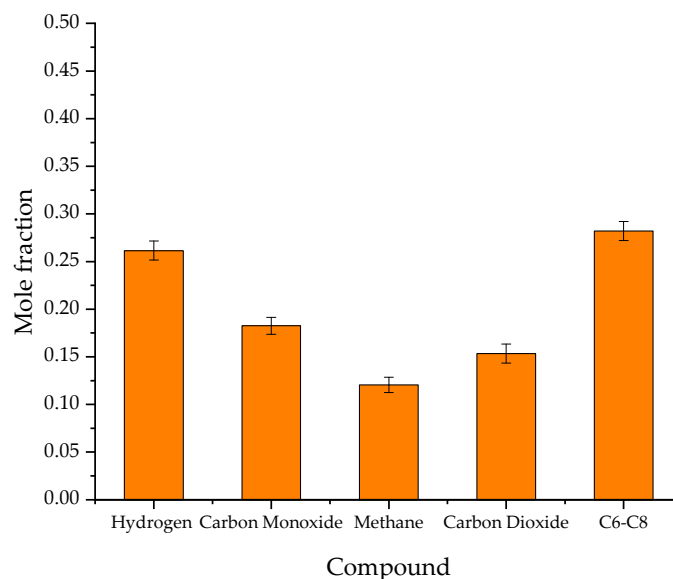
Figure A1. Product mole fractions from 2M4MP thermal gasification on a dry basis. Thermal runs without a loaded catalyst are evaluated using a 2M4MP, as follows: S/2M4MP = 1.5 g/g, reaction time= 20 s, temperature = 600 °C.

Figure 6 reports that thermal 2M4MP gasification at 600 °C yields a significant fraction of C6–C8 species, with a 50% 2M4MP conversion. This 50% 2M4MP conversion is smaller than the 80% 2M4MP conversion from catalytic gasification runs. Furthermore, the thermal runs yield significant fractions of C6–C8, which are much larger in quantity than those obtained from the catalytic runs.

Appendix B. Product Mole Fractions at Different Temperatures for Cat A and Cat B

Figures A2 and A3 report the product mole fraction at different temperatures for both Cat A and Cat B, respectively.
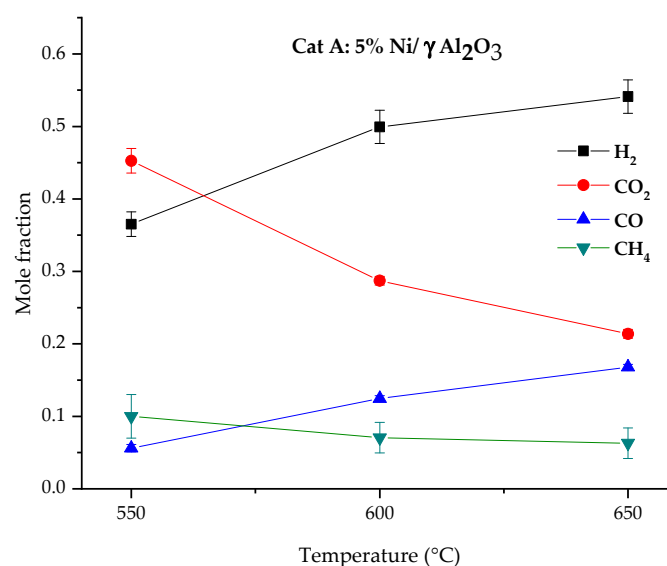

Figure A2. Product mole fractions reported on a dry basis using Cat A: 5%Ni/γAl$_2$O$_3$ at 550 °C, 600 °C and 650 °C, a S/2M4MP = 1.5 g/g and 20 s reaction time. Reported values are the average of at least three repeats.

Figure A3. Product Mole Fractions on a Dry Basis using Cat B: 5%Ni-0.25%Ru/γAl_2O_3 at 550 °C, 600 °C and 650 °C, a S/2M4MP = 1.5 g/g, 20 s reaction time. Reported values are the average of at least three repeats.
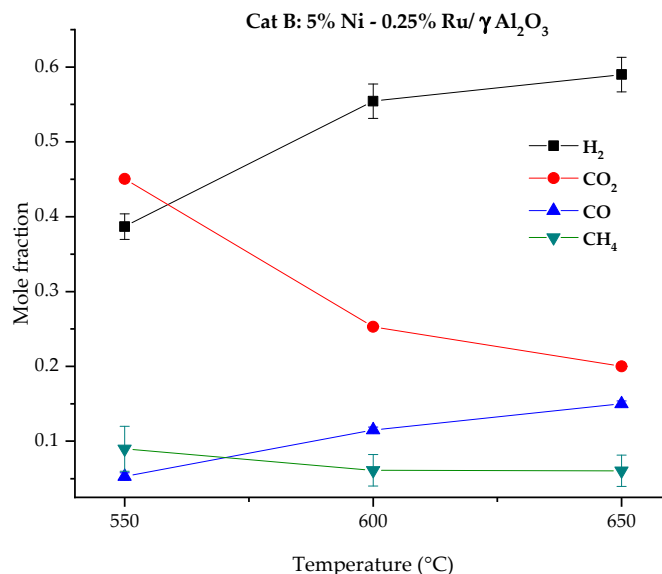
One can observe that higher temperatures for both Cat A and Cat B display: (a) higher hydrogen mole fractions, (b) lower CO_2 mole fractions, (c) higher CO mole fractions and (d) lower methane. Thus, one can speculate that, at higher temperatures, both the water–gas shift reaction (CO + $H_2O \rightarrow$ CO_2 + H_2) and methane reforming are favored (CH_4 + $H_2O \rightarrow$ CO + $3H_2$).

References

1. Mao, G.; Huang, N.; Chen, L.; Wang, H. Research on biomass energy and environment from the past to the future: A bibliometric analysis. *Sci. Total Environ.* **2018**, *635*, 1081–1090. [CrossRef] [PubMed]
2. Nunes, L.J.R.; Causer, T.P.; Ciolkosz, D. Biomass for energy: A review on supply chain management models. *Renew. Sustain. Energy Rev.* **2020**, *120*, 109658. [CrossRef]
3. Ren, J.; Cao, J.-P.; Zhao, X.-Y.; Yang, F.-L.; Wei, X.-Y. Recent advances in syngas production from biomass catalytic gasification: A critical review on reactors, catalysts, catalytic mechanisms and mathematical models. *Renew. Sustain. Energy Rev.* **2019**, *116*, 109426. [CrossRef]
4. Li, D.; Tamura, M.; Nakagawa, Y.; Tomishige, K. Metal catalysts for steam reforming of tar derived from the gasification of lignocellulosic biomass. *Bioresour. Technol.* **2015**, *178*, 53–64. [CrossRef]
5. Guan, G.; Kaewpanha, M.; Hao, X.; Abudula, A. Catalytic steam reforming of biomass tar: Prospects and challenges. *Renew. Sustain. Energy Rev.* **2016**, *58*, 450–461. [CrossRef]
6. Guan, G.; Chen, G.; Kasai, Y.; Lim, E.W.C.; Hao, X.; Kaewpanha, M.; Abuliti, A.; Fushimi, C.; Tsutsumi, A. Catalytic steam reforming of biomass tar over iron- or nickel-based catalyst supported on calcined scallop shell. *Appl. Catal. B Environ.* **2012**, *115*, 159–168. [CrossRef]
7. De Lasa, H.; Salaices, E.; Mazumder, J.; Lucky, R. Catalytic Steam Gasification of Biomass: Catalysts, Thermodynamics and Kinetics. *Chem. Rev.* **2011**, *111*, 5404–5433. [CrossRef]
8. Mazumder, J.; de Lasa, H.I. Catalytic steam gasification of biomass surrogates: Thermodynamics and effect of operating conditions. *Chem. Eng. J.* **2016**, *293*, 232–242. [CrossRef]
9. Vera, D.; Jurado, F.; Carpio, J.; Kamel, S. Biomass gasification coupled to an EFGT-ORC combined system to maximize the electrical energy generation: A case applied to the olive oil industry. *Energy* **2018**, *144*, 41–53. [CrossRef]
10. Claude, V.; Courson, C.; Köhler, M.; Lambert, S.D. Overview and Essentials of Biomass Gasification Technologies and Their Catalytic Cleaning Methods. *Energy Fuels* **2016**, *30*, 8791–8814. [CrossRef]
11. Abu El-Rub, Z.; Bramer, E.A.; Brem, G. Review of Catalysts for Tar Elimination in Biomass Gasification Processes. *Ind. Eng. Chem. Res.* **2004**, *43*, 6911–6919. [CrossRef]

12. Ashok, J.; Kathiraser, Y.; Ang, M.L.; Kawi, S. Bi-functional hydrotalcite-derived $NiO–CaO–Al_2O_3$ catalysts for steam reforming of biomass and/or tar model compound at low steam-to-carbon conditions. *Appl. Catal. B Environ.* **2015**, *172*, 116–128. [CrossRef]

13. Mazumder, J.; de Lasa, H.I. Ni catalysts for steam gasification of biomass: Effect of La_2O_3 loading. *Catal. Today* **2014**, *237*, 100–110. [CrossRef]

14. Xiao, X.; Liu, J.; Gao, A.; Zhouyu, M.; Liu, B.; Gao, M.; Zhang, X.; Lu, Q.; Dong, C. The performance of nickel-loaded lignite residue for steam reforming of toluene as the model compound of biomass gasification tar. *J. Energy Inst.* **2018**, *91*, 867–876. [CrossRef]

15. Liu, H.; Wang, B.; Fan, M.; Henson, N.; Zhang, Y.; Towler, B.F.; Gordon Harris, H. Study on carbon deposition associated with catalytic CH_4 reforming by using density functional theory. *Fuel* **2013**, *113*, 712–718. [CrossRef]

16. Lee, S.; Bae, M.; Bae, J.; Katikaneni, S.P. Ni–Me/Ce0.9Gd0.1O_2−x (Me: Rh, Pt and Ru) catalysts for diesel pre-reforming. *Int. J. Hydrog. Energy* **2015**, *40*, 3207–3216. [CrossRef]

17. Crisafulli, C.; Scirè, S.; Maggiore, R.; Minicò, S.; Galvagno, S. CO_2 reforming of methane over Ni–Ru and Ni–Pd bimetallic catalysts. *Catal. Lett.* **1999**, *59*, 21–26. [CrossRef]

18. Iida, H.; Fujiyama, A.; Igarashi, A.; Okumura, K. Steam reforming of toluene over $Ru/SrCO_3$-Al_2O_3 catalysts. *Fuel Process. Technol.* **2017**, *168*, 50–57. [CrossRef]

19. Katheria, S.; Deo, G.; Kunzru, D. Rh-Ni/$MgAl_2O_4$ catalyst for steam reforming of methane: Effect of Rh doping, calcination temperature and its application on metal monoliths. *Appl. Catal. A Gen.* **2019**, *570*, 308–318. [CrossRef]

20. Tomishige, K.; Asadullah, M.; Kunimori, K. Syngas production by biomass gasification using $Rh/CeO_2/SiO_2$ catalysts and fluidized bed reactor. *Catal. Today* **2004**, *89*, 389–403. [CrossRef]

21. Zhang, R.; Liu, H.; Li, Q.; Wang, B.; Ling, L.; Li, D. Insight into the role of the promoters Pt, Ru and B in inhibiting the deactivation of Co catalysts in Fischer-Tropsch synthesis. *Appl. Surf. Sci.* **2018**, *453*, 309–319. [CrossRef]

22. Li, S.; Gong, D.; Tang, H.; Ma, Z.; Liu, Z.-T.; Liu, Y. Preparation of bimetallic Ni@Ru nanoparticles supported on SiO_2 and their catalytic performance for CO methanation. *Chem. Eng. J.* **2018**, *334*, 2167–2178. [CrossRef]

23. González, C.D.G.; Sanchez, E.A.; Cruz, R.I.; Calzada, H.A.R.; Serrano, R.B. Catalytic Steam Gasification of Glucose for Hydrogen Production Using Stable Based Ni on a γ–Alumina Fluidizable Catalyst. *Int. J. Chem. React. Eng.* **2019**, *17*. [CrossRef]

24. Mazumder, J.; de Lasa, H.I. Fluidizable La_2O_3 promoted Ni/γ-Al_2O_3 catalyst for steam gasification of biomass: Effect of catalyst preparation conditions. *Appl. Catal. B Environ.* **2015**, *168*, 250–265. [CrossRef]

25. Sharma, S.; Hines, L. Oxidation of Ruthenium. *IEEE Trans. Compon. Hybrids Manuf. Technol.* **1983**, *6*, 89–92. [CrossRef]

26. Mazumder, J.; de Lasa, H.I. Steam gasification of a cellulosic biomass surrogate using a Ni/La_2O_3-γAl_2O_3 catalyst in a CREC fluidized riser simulator. Kinetics and model validation. *Fuel* **2018**, *216*, 101–109. [CrossRef]